Estimation of Restoring Force Characteristics in the Interior Beam-and-Column Subassemblages of R/C Frames

Masaru Teraoka, Kazuya Hayashi
Satoshi Sasaki, Naoki Takamori

Abstract

The objectives of this study were to investigate seismic behavior and restoring force characteristics of interior beam-and-column subassemblages using normal-to high-strength materials. Initially, cyclic loading tests were carried out on sixteen half-scale interior beam-and-column subassemblages using high-strength materials, in order to investigate their seismic behavior. Subsequently, multiple regression analysis, taking the various factors into account, was carried out to estimate the restoring force characteristics of subassemblages. In the multiple regression analysis, the test data of this study and authors' previous work using normal-strength materials were used.

The following statements can be made from this study;

(1) The anchorage capacity of beam longitudinal bars passing through the interior beam-column joint affects the energy absorption of a frame.

(2) The plastic deformation performance of subassemblages of a beam yielding frame is greatly effected by the joint input shear force level and the amount and strength joint shear reinforcement.

(3) A method to estimate restoring force characteristics of the subassemblages that takes the above effects into account was developed. The results calculated by the proposed method closely predicted the ductility performance and hysteresis characteristics measured in the test subassemblages.

§1. Introduction

To estimate the seismic behavior of the R/C ductile moment-resisting frames, it is important to clarify the effect of anchorage performance of beam longitudinal bars passing through the interior beam-column joint and the joint shear stress level on restoring force characteristics of the frame[1),2)].The main objectives of this study were to investigate seismic behavior and to estimate restoring force characteristics of interior beam-and-column subassemblages using normal-to high-strength materials.

Keywords： R/C frame; restoring force characteristic; ductility performance; estimation; normal-to high-strength material; interior beam-and-column subassemblage

Initially, sixteen half-scale cyclic loading tests were carried out on interior beam-and-column subassemblages using high-strength materials to investigate their seismic behavior. We also carried out, multiple regression analysis, taking the various factors into account, in order to estimate the restoring force characteristics of subassemblages. In the multiple regression analysis, the test data of this study and authors' previous work using normal-strength materials were used. Some of this work has already been published [3),4)].

§2. Detail of Test Units and Testing Procedure

2.1 Specimens and the Used Materials

Sixteen half- scale model specimens were tested. Their cross-sectional properties are detailed in Tab. 1. Typical configuration of the specimen is shown in Fig.1. The primary variables were:

1) compressive strengths of the concrete (f_c') were 55,90,110and140N/mm²,
2) yield strengths of the beam longitudinal reinforcement (${}_bf_y$) were 382 to 858N/mm²,
3) nominal joint shear stress levels (v_n) at beam flexural yielding of 7.0 to 29.1 N/mm²,
4) bond index ($\mu={}_bf_y \cdot {}_db_d/(D_c \cdot \sqrt{f_c'})$, where ${}_db_d$ is bar diameter and D_c is column depth) levels of 7.9 to 17.7.

Test specimens were separated in to six groups. For group Ⅰ, Ⅱ and Ⅲ, the design joint shear stress levels were 7.5, 11.0 and 15.5 N/mm² respectively. In this paper, the effective area in joint is defined as $b_c \cdot j_c$ at shear cracking and $(b_b+b_c) \cdot j_c /2$ at ultimate state. Where, b_b is beam width, b_c is column width and j_c is 7/8th of effective depth of the column. The grade of ${}_bf_y$, their diameter and number of beam bars in each group were changed to give different value of μ from 7.9 to 17.7. For specimens of group Ⅳand Ⅴ, the levels of v_n were varied from 15.1 to 29.1N/mm². The specimens HJ-11 and HJ-12, HJ-12 and HJ-14 have different ${}_bf_y$ and f_c'. The specimens of group Ⅵ were constructed by using precast beams and columns. The compressive strength of the concrete was 140N/mm² in columns and joints, and 75N/mm² in beams. The specimens HJ-15 and HJ-16 have different level of v_n.

Table 2 shows the mechanical properties of concrete and reinforcement respectively.

2.2 Test Method

As shown in Fig.1, the column was supported by pins and hinges at the top and bottom ends and subjected to constant axial load, while beams were subjected to lateral loading reversals.

Tab. 1 Details of test subassemblages

Group		Ⅰ			Ⅱ			Ⅲ			Ⅳ			Ⅴ		Ⅵ	
Specimen		HJ-1	HJ-2	HJ-3	HJ-4	HJ-5	HJ-6	HJ-7	HJ-8	HJ-9	HJ-10	HJ-11	HJ-12	HJ-13	HJ-14	HJ-15	HJ-16
H×L		2,000×3,000 mm (Story height × Span Length)									1,800×2,800 mm					2,000×3,000 mm	
Concrete		fc'≒55 N/mm²						fc'≒90 N/mm²						fc'≒110 N/mm²		fc'≒140N/mm²(Column,Joint) fc'=75N/mm2(Beam)	
Beam	Section	$b_b \times D_b$=300×400(=Width×Depth of Beam(mm×mm))														320×450	
Beam, Main Bars	Top/Bot.	4-D19	4-HD16	2-UD19	6-D19	4-HD19	3-UD19	6-D22	4-HD22	4-UD19	8-HD16	8-D22	8-HD22	4-HD19 4-HD16	8-HD22	4-UD22	6-UD22
Beam, Main Bars	a_t(cm²)	1148	796	574	1722	1148	861	2322	1548	1148	1592	3096	3096	1944	3096	1548	2322
Beam, Main Bars	${}_bp_t$(%)	1.08	0.75	0.54	1.69	1.08	0.81	2.28	1.45	1.08	1.63	3.13		1.99	3.13	1.21	1.9
Beam, Main Bars	${}_bf_y$(N/mm²)	382	624	858	382	645	858	422	599	858	611	441	604	634 611	604	786	786
Beam, Main Bars	$a_t \cdot {}_bf_y$(kN)	439	496	493	659	741	739	979	928	985	973	1366	1870	1211	1870	1216	1824
Beam	Stirrups	▥-D6		□-D10	▥-HD6		◫-HD6	▥-HD6								▥-UD8	
Beam, End	@(mm)	75		85	100		75	75			80	60	50	60	50	70	50
Beam, End	p_w(%)	0.57		0.56	0.43		0.43	0.57			0.53	0.71	0.85	0.71	0.85	0.89	1.25
Beam, Other	@(mm)	100		110	120		90	90			100	75	50	75	50	70	50
Beam, Other	p_w(%)	0.43		0.43	0.36		0.36	0.47			0.39	0.57	0.85	0.57	0.85	0.89	1.25
Column	Section	$b_c \times D_c$=40×40(=Width×Depth of Column(cm×cm))														450×450	
Column	Main Bars	12-D19(${}_cf_y$=382N/mm²)			12-HD19(${}_cf_y$=645N/mm²)						8-HD22 4-HD19	8-D22 4-D19	8-HD22 (${}_cf_y$=604N/mm²) 4-HD19 (${}_cf_y$=634N/mm²)			12-UD22(${}_cf_y$=786N/mm²)	
Column	a_g,p_g,${}_cp_t$	a_g=3444mm²,p_g=2.15%,${}_cp_t$=0.72%									a_g=4243mm²,p_g=2.65%,${}_cp_t$=0.84%					a_g=8514mm²,p_g=4.20%,${}_cp_t$=0.76%	
Column	Hoops	⬡-D10@100,p_w=0.71%									⬡-D10@50,p_w=1.42%					⬡UD8@40,p_w=0.89%	
Joint	Hoops	□-D10@50,p_w=0.71%						⬡-HD8@50,p_w=1.0%								□-UD8@40,p_w=0.56%	
Joint	v_n(N/mm²)	7.02	7.93	7.87	10.59	11.87	11.77	15.79	14.81	15.79	15.10	21.28	29.13	18.83	29.13	15.40	23.34
Joint	v_{ju}(N/mm²)	12.45	12.85	12.85	14.32	14.51	14.51	19.71	19.52	19.81	20.69	22.75	25.11	24.03	27.36	23.14	26.58
Joint	v_n/v_{ju}	0.56	0.62	0.61	0.74	0.82	0.82	0.80	0.76	0.79	0.73	0.93	1.16	0.79	1.06	0.67	0.88
D_c/d_{bd}		21.1	25.0	21.1	21.1	21.1	21.1	18.2	18.2	21.1	25.0	18.2	18.2	21.1	18.2	20.50	20.50
u_b(N/mm²)		9.08	12.47	20.38	9.08	15.33	20.38	11.60	16.48	20.38	12.26	12.16	16.57	15.10	16.57	19.21	19.21
μ		7.88	10.82	17.67	7.88	13.29	17.67	7.70	10.94	13.53	8.31	8.25	11.24	8.92	9.79	10.41	10.41
$\Sigma M_{cu}/\Sigma M_{bu}$		3.01	2.66	2.68	2.60	2.22	2.22	2.42	2.45	2.30	2.51	1.58	1.30	2.00	1.32	3.56	2.43
f_o(N/mm²)		9.81						17.65			14.71					28.05	
η_o		0.181						0.191			0.166			0.126		0.202	

Note: For the meaning of symbols, see appendix Ⅰ.

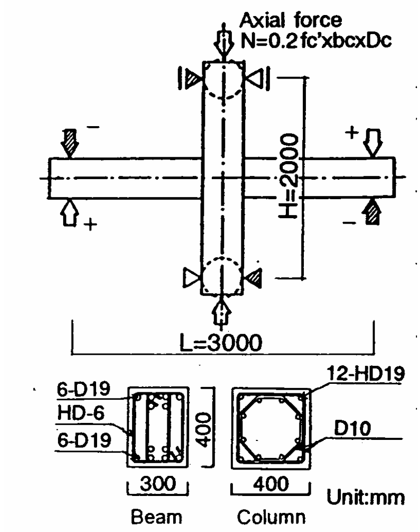

Fig. 1 Typical specimen details (HJ−4)

Tab. 2 Mechanical properties of materials

(a) Concrete

Group	Member	fc'	E
Ⅰ	Beam Joint	54.2	28.7
Ⅱ	Column	54.3	30.8
Ⅲ	Beam Joint	92.6	38.4
	Column	83.4	38.0
Ⅳ	Beam Joint	88.7	36.6
	Column	93.8	39.5
Ⅴ	Beam Joint	116.9	38.0
	Column	107.6	36.4
Ⅵ	Beam	75.5	33.4
	Joint	138.2	43.5
	Column	146.3	40.9

Note: Test results are average values of five sealed cylinders (200mm high × 100nm dia.)

fc'=Compressive strength(N/mm²)
E=Young's modulus at 1/4fc'(kN/mm²)

(b) Reinforcement

Group	Type	a	f_y
Ⅰ ~ Ⅲ	HD22	387	599
	D22	387	422
	UD19	287	858
	HD19	287	645
	D19	287	382
	HD16	199	624
	D10	71	347
	UD8	50	797 *
	UD6	32	762 *
	D6	32	312
Ⅳ Ⅴ	HD22	387	604
	D22	387	441
	HD19	287	634
	D19	287	442
	HD16	199	611
	D10	71	343
	HD8	50	681 *
	UD6	32	827 *
Ⅵ	UD22	387	776
	UD8	50	986

Note ＊: Value based on 0.2% offset
a=Nominal cross sectional area (mm²)
f_y=Yield strength (N/mm²)

§3. Test Results and Discussion

3.1 Outline of Test Results

Table 3 shows the basic experimental results. Figure 2 shows the relations between story shear force (Q_c) and interstory drift angle (R_T). Fig. 3 illustrates the typical crack patterns of beam-column joints at the final loading stage. Fig. 4 shows the relation between joint input shear stress levels (v_n/v_{ju}) and ultimate interstory drift angles (R_{Tu}). Where, v_{ju} is the calculated ultimate joint shear strength using the equation proposed by the authors[5)] , and R_{Tu} is defined as the interstory drift angle that can maintain the story shear force (Q_{cby})

Tab.3 Test results on measured and calculated values

Group	Specimen	Flex. yielding in beam Q_{cby} (kN)	Q_{cbu} (kN)	R_{Ty} (10^{-3})	Maximum load Q_{cm} (kN)	Q_{cbm} (kN)	R_{Tm} (10^{-3})	Ult.story drift R_{Tu} (10^{-3})	${}_cR_{Tu}$ (10^{-3})	Shear cracking in joint v_{jc} (N/mm²)	${}_cv_{jc}$ (N/mm²)	Maximum stress in joint v_{jm} (N/mm²)	v_{ju} (N/mm²)	Max. ave. bond stress u_{avm} (N/mm²)	${}_cu_{avm}$ (N/mm²)	Equivalent viscous damping ratio h_{eq} (%) R_T=1/100 Exp.	R_T=1/100 Cal.	R_T=2/100 Exp.	R_T=2/100 Cal.	R_T=3/100 Exp.	R_T=3/100 Cal.	Failure mode
Ⅰ	HJ-1	148	157	3.9	197	187	36.9	70.2	65.5	6.8	7.1	8.9	−	10.3	8.5	17.1	12.7	23.9	26.7	22.8	26.7	F
	HJ-2	169	178	6.8	220	210	34.7	58.8	58.0	7.2	7.1	9.9	−	13.0	11.5	6.41	7.27	15.9	14.8	17.6	17.0	F
	HJ-3	178	176	10.9	197	210	24.8	40.3	58.7	6.7	7.1	9.0	−	17.3	15.2	4.53	4.56	14.0	11.7	15.8	13.3	FB
Ⅱ	HJ-4	196	225	5.5	253	253	16.7	40.1	45.8	7.0	7.1	12.5	14.3	10.5	8.5	8.55	10.2	17.9	20.5	15.7	20.5	FS
	HJ-5	253	264	10.0	296	299	16.4	42.4	40.4	6.7	7.1	13.4	14.5	15.5	12.5	4.40	5.22	10.8	9.80	12.8	12.6	FS
	HJ-6	255	263	12.7	286	298	20.9	36.5	40.5	6.9	7.1	13.0	14.5	18.6	15.2	4.62	3.72	9.3	9.84	11.8	13.2	FS(B)
Ⅲ	HJ-7	279	332	5.7	376	387	22.2	57.1	60.1	9.9	10.4	18.4	19.7	13.1	11.3	7.18	7.82	17.9	15.4	18.2	20.5	FS
	HJ-8	352	331	10.0	395	387	29.9	63.3	64.4	9.9	10.4	17.9	19.5	18.0	14.6	4.42	5.39	14.0	10.3	16.0	13.9	FS
	HJ-9	329	350	11.4	382	407	21.3	46.8	60.7	9.0	10.4	17.4	19.8	21.3	17.9	4.20	3.67	10.2	10.1	15.2	13.0	FB(S)
Ⅳ	HJ-10	369	354	9.3	444	404	29.8	80.0	63.0	11.2	9.2	19.1	20.7	11.5	12.7	4.71	5.58	12.2	11.3	15.7	15.6	FS
	HJ-11	510	500	10.4	581	537	24.2	43.5	46.1	11.0	9.2	25.2	22.8	12.1	11.1	5.10	5.92	11.8	11.3	16.1	16.3	FS
	HJ-12	642	683	15.9	681	625	24.3	25.0	34.7	11.4	9.2	29.5	25.1	15.6	13.9	4.55	3.49	8.00	6.21	−	−	FS
Ⅴ	HJ-13	458	454	12.0	541	516	35.0	76.0	57.5	11.4	10.1	22.8	24.0	12.5	15.0	3.76	4.63	8.24	9.04	13.2	13.4	FS
	HJ-14	632	686	17.0	714	668	29.3	32.5	38.8	8.4	10.1	30.8	27.4	16.1	15.3	3.76	3.73	5.38	6.84	12.5	11.3	FS
Ⅵ	HJ-15	536	484	9.7	613	610	34.4	45.0	65.8	13.1	13.7	19.3	−	22.5	18.8	3.88	4.49	10.9	8.81	13.5	12.7	F(S)
	HJ-16	730	692	12.1	835	819	29.7	41.0	45.9	16.1	13.7	27.9	26.6	18.8	18.8	3.71	3.58	7.08	6.75	12.5	11.0	FS

Notes: Q_{cby}=measured story shear at beam yielding, Q_{cbu}=calculated story shear at beam yielding according to the AIJ (1988), R_{Ty}=measured story drift angle at beam flexural yielding, Q_{cm}=measured story shear at maximum load, Q_{cbm}=calculated story shear at beam maximum capacity according to the eq. by the authors (1996). R_{Tm}=measured story drift angle at maximum load, R_{Tu}=measured ultimate story drift angle, ${}_cR_{Tu}$=calculated ultimate story drift angle according to eq.(1), v_{jc}=measured shear cracking stress in joint, ${}_cv_{jc}$=calculated shear cracking stress in joint based on the principal stress equation, v_{jm}=measured maximum stress in joint, v_{ju}=calculated ultimate shear strength according to the eq. by the authors (1991), u_{avm}=measured maximum value on average bond stress of beam main bar in joint, ${}_cu_{avm}$=calculated values according to eq. (2), F mode=beam end flexural compression failure after beam flexural yielding, FB-mode=beam end flexural compression failure due to considerable slippage of beam longitudinal bars in joint region after beam flexural yielding, FS mode=joint shear failure after beam flexural yielding.

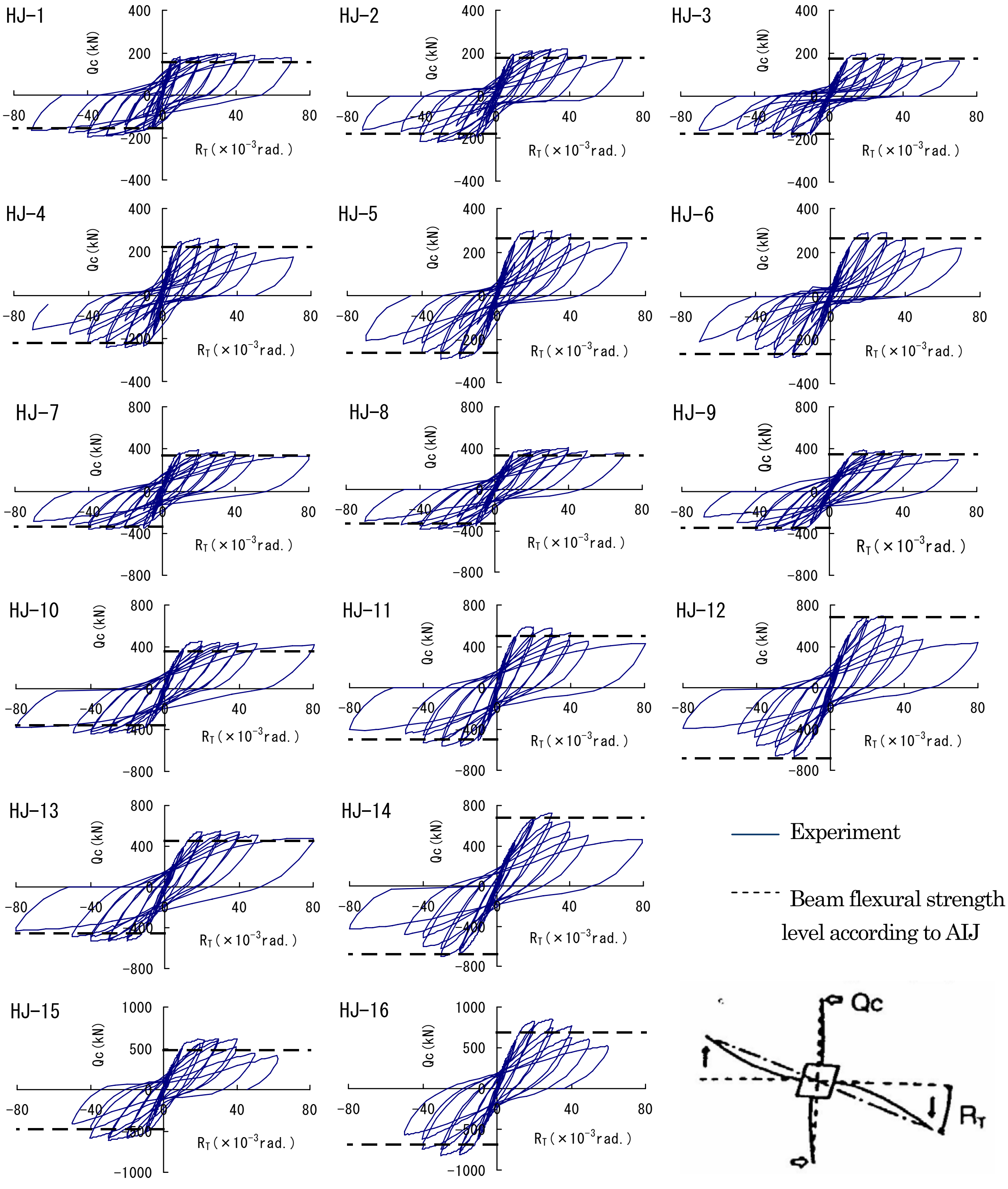

Fig. 2 Story shear (Q_c)—interstory drift angle (R_T) hysteresis characteristics

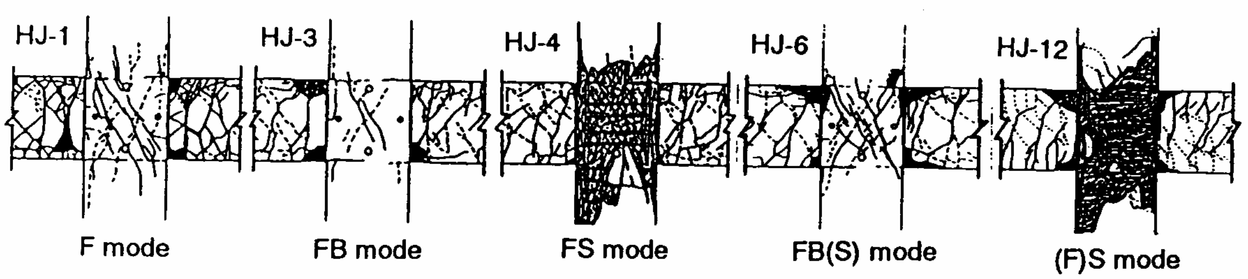

Fig. 3 Typical crack patterns at final loading stage

corresponding to the calculated beam flexural yield strength by the approximate equation of the AIJ (1988)[6] on the Q_c-R_T envelope curve as shown in Fig.5. The equivalent viscous damping ratio (h_{eq}) of second hysteresis loop at each interstory drift angle and for each specimen of group Ⅰ, Ⅱ and Ⅲ are shown in Fig.6.

3.2 Failure Mode and Restoring Force Characteristics

All specimens attained maximum strength after flexural yielding of beams. The final failure modes were influenced by the levels of v_n and μ. The interstory drift angle (R_{Ty}) at beam flexural yielding became large in respect of high μ and v_n/v_{ju} values (see Tabs. 1 and 3). On the other hand, the values of R_{Tu} become large for the specimens with low μ and low v_n/v_{ju} (see Fig.4 and Tab. 1).

In group Ⅰ (v_n≒7.5N/mm²), HJ-1 and HJ-2 with lower μ value showed F mode (beam end flexural compression failure after beam flexural yielding), HJ-3 with higher μ value (μ=17.7) showed FB mode (beam end flexural compression failure due to considerable slippage of beam bars in joint region after beam flexural yielding). For the specimens with F mode, the interstory drift angles (R_{Tm}) at maximum load were about 35×10⁻³rad., and thereafter the capacity decreased gradually. But in the case of the specimens failing in FB mode, the slippage of beam longitudinal bars became large after their yielding, the value of R_{Tm} was 25×10⁻³rad., and the hysteresis loop indicated slightly poor energy dissipation capacity.

In group Ⅱ and Ⅲ (v_n≒11.0, 15.5N/mm²), shear deterioration of beam-to-column joint progressed to some extent at interstory drift angles 20 to 30×10⁻³rad. after beam flexural yielding. The specimens HJ-4, HJ-5, HJ-7 and HJ-8 with lower μ values showed FS mode (joint shear failure after beam flexural yielding), and the specimens HJ-6 and HJ-9 with higher μ values showed FB(S) mode (FB mode with slightly joint shear deterioration). These specimens showed the beam-end crushing and rapid slippage of beam longitudinal bars in joints at interstory drift angles of 30 to 40×10⁻³rad.. In comparison to the specimens in groups Ⅱ and Ⅲ, the specimens in group Ⅲ with high strength concrete showed superior restoring force characteristics.

For groups Ⅳ to Ⅵ, specimens showed FS failure mode (except HJ-15 which showed F(S) mode (F mode with slightly joint shear deterioration)). But the failure intensity and hysteresis behavior were different according to v_n. At maximum load, the specimen HJ-12 and HJ-14 suffered concrete crush in the joint and shear crack enlarged in the column region resulting

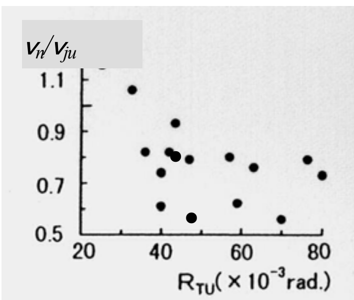

Fig. 4 v_n/v_{ju} and R_{Tu} relations

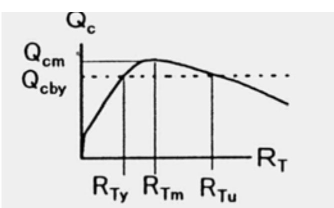

Fig.5 Definition of ultimate interstory drift angle (R_{Tu})

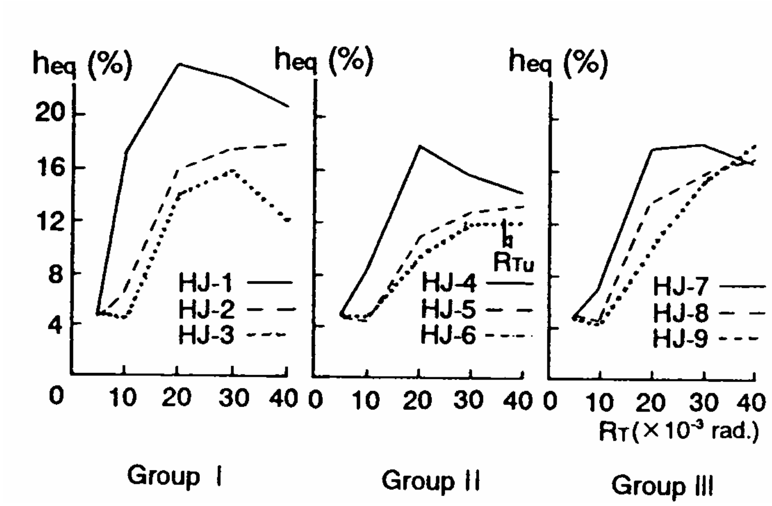

Fig. 6 Comparison of h_{eq}—R_T relationships

in concrete splitting. These behaviors were not observed in the case of specimens HJ-10, HJ-13 and HJ-15. The R_{Tm} values of their specimens were in the range of 25 to 35×10^{-3}rad.. Specimens HJ-10 and HJ-13, whose v_n were lower, showed stable hysteresis response even at $R_T > 50\times10^{-3}$rad. followed by maximum load. The specimens HJ-12 and HJ-14, which were provided with higher v_n, showed less ductile response. At maximum load, the joint shear stresses (v_{jm}) of specimens HJ-12 and HJ-14 were 29.5 and 30.8 N/mm^2 respectively. In comparison to the specimens in groups Ⅳ to Ⅵ, the specimens in group Ⅵ showed slightly worse restoring force characteristics.

The limit of beam longitudinal bars passing through interior beam-column joint should be based on not only the value of μ but also the joint shear stress level v_n.

3.3 Strength

In Table 3, the measured capacities at beam flexural yielding and at maximum load are compared with the calculated values. The ratio of the measured flexural yielding capacities (Q_{cby}) to the calculated values (Q_{cbu}) by the approximate equation of AIJ (1988)[6] varied between 0.84 ~~to~~ and 1.10 (average 0.98). The ratio of the measured maximum capacities (Q_{cm}) to the calculated values (Q_{cbm}) by the formula proposed by the authors[7] varied between 0.94 and 1.10 (average 1.02).

In Table 3, the shear cracking strengths of the joint panels, calculated by the principal stress equation (${}_cv_{jc}$), taking the tensile strength of concrete f_t=0.50 $\sqrt{f_c'}$ (unit:N/mm^2) into account, are compared with the measured values (v_{jc}). The ratios $v_{jc}/{}_cv_{jc}$ were 0.83 to 1.23 (average 1.02). The calculated values of v_{ju} are compared with the measured maximum joint shear stresses (v_{jm}). The ratio v_{jm}/v_{ju} of the specimens for FS mode was 0.87 to 1.17 (average 0.98). The estimated values of joint shear cracking strength and ultimate strength are in good agreement with measured values.

§4. Estimation of Ultimate Interstory Drift Angle

4.1 Available Specimens

In addition to the sixteen specimens of this study, twenty-seven specimens using normal-strength materials tested previously by the authors[3] are used for the study of estimation of R_{Tu}. The properties of twenty-seven specimens are detailed in Table 4.

4.2 Estimation of Ultimate Interstory Drift Angle

In the range after maximum load, flexural deformation of the beam ends and shear deterioration of the joint panel are linked in a complex manner, and bond deterioration in the longitudinal bars and additional deformation of the members becomes more pronounced. Due to these influences, estimation of the deformation capacities of each member is difficult. In this paper, a statistical method was used.

Statistical analysis showed that R_{Tu} is strongly affected by the ratio v_n/v_{ju} as well as by $p_w\cdot{}_wf_y$. The relationships between R_{Tu} and v_n/v_{ju} and between R_{Tu} and $p_w\cdot{}_wf_y$ are shown in Fig.7. The following regression equation for R_{Tu} was obtained statistically:

$$ {}_cR_{Tu}=0.0326\,(0.763+0.0076p_w\cdot{}_wf_y)\cdot(v_n/v_{ju})^{-1.30} \qquad (1) $$

where of $p_w\cdot{}_wf_y$ is expressed in N/mm^2. A comparison between calculated the value by eq.(1) and measured values (R_{Tu}) is shown in Fig. 8 and Table. 3. They show good agreement.

§5. Relations Between Bond Stress Characteristics and Equivalent Viscous Damping Factors

The maximum values on average bond stress (u_{avm}) of beam longitudinal bars in the joint, which represent the bond characteristics, is studied first

Tab. 4 Concerned specimens using normal-strength materials[3)]

Specimen	H × L (mm)	f_c'* (N/mm²)	Beam: b_b × D_b (mm)	Beam: $_bp_t$ (%)	Beam: $_bf_y$ (N/mm²)	Column: b_c × D_c (mm)	Column: $_cp_t$ (%)	Column: $p_w \cdot {}_wf_y$ (N/mm²)	Column: $\frac{v_n}{v_{ju}}$	Bond: $\frac{D_c}{d_{bd}}$	Bond: u_b (N/mm²)	Bond: μ	R_{Tu} (x10⁻³)	Failure Modes
NO.6	1,300	F39.6	240	2.48	411	300	0.9	4.25	1.02	13.6	15.1	15.3	23.5	FS
NO.7	×	46.8	×	2.48	411	×	0.9	4.25	1.04	13.6	15.1	14.1	27.2	FS
NO.8	2,500	46.8	300	2.48	411	300	0.9	6.18	1.04	13.6	15.1	14.1	32.8	FS
NO.13	1,300	L32.0	275	1.25	406	375	0.7	4.64	0.82	19.7	10.3	11.6	45.6	F
NO.14	×	29.4	×	1.46	433	×	0.8	4.64	0.89	17.0	12.7	13.6	49.5	F
NO.15	2,500	29.4	375	1.46	433	375	0.8	4.64	0.89	17.0	12.7	13.6	48.7	F
NO.16		30.8		1.29	431		0.35	3.60	0.79	23.7	9.0	10.4	65.3	F
NO.17	1,100	30.8	260	1.47	431	380	0.35	3.60	0.77	23.7	9.0	10.4	47.0	F
NO.18	×	30.8	×	1.55	438	×	0.35	3.60	0.84	20.0	11.0	12.6	45.5	F
NO.19	2,000	30.8	320	1.85	417	380	0.35	3.60	0.94	17.3	12.1	13.9	47.5	FS
NO.20		30.8		2.13	417		0.35	3.60	1.01	17.3	12.1	13.9	39.8	FS
NO.21		L25.2		1.19	426		0.69	1.95	0.85	26.2	8.1	10.4	39.3	FS
NO.22		L26.7		1.63	426		0.69	1.95	1.01	26.2	8.1	10.1	22.4	FS
NO.23	1,100	34.0	260	1.63	426	340	0.69	1.95	0.81	26.2	8.1	8.9	43.5	FS
NO.24	×	39.4	×	0.96	601	×	0.69	1.95	0.68	21.3	14.1	14.4	42.9	F
NO.25	2,160	F37.5	300	0.96	601	340	0.69	1.95	0.63	21.3	14.1	14.8	39.3	F
NO.26		35.6		2.09	399		0.69	1.95	0.90	21.3	9.4	10.1	36.3	FS
NO.27		F32.2		2.09	399		0.69	1.95	0.86	21.3	9.4	10.6	36.9	FS
NO.29		44.0		2.09	399		0.69	1.95	0.78	21.3	9.4	9.0	33.0	FS
NO.31	2,000	31.9	365	1.57	421	540	0.79	1.97	0.78	21.6	9.7	11.0	43.7	FS
NO.32	×	33.7	×		421	×	0.79	1.84	0.75	21.6	9.7	10.7	46.0	FS
NO.33	3,150	34.7	560	(1.10)	421	540	0.79	3.30	0.71	21.6	9.7	10.6	45.7	FS
NO.34		39.4		1.50	429		0.54	2.41	0.78	20.0	10.7	10.9	39.4	FS
NO.35	2,000	39.4	300	1.50	429	500	0.54	2.41	0.78	20.0	10.7	10.9	36.6	FS
NO.36	×	39.4	×	1.84	429	×	0.54	2.41	0.89	20.0	10.7	10.9	31.9	FS
NO.37	3,500	39.4	500	1.50	429	500	0.54	2.41	0.85	20.0	10.7	10.9	39.6	FS
NO.38		39.4		1.50	429		0.54	2.41	0.85	20.0	10.7	10.9	29.3	FS

Notes: ∗L=light weight concrete, F=steel fiber reinforced concrete, For the meanings of other symbols, see appendix Ⅰ.

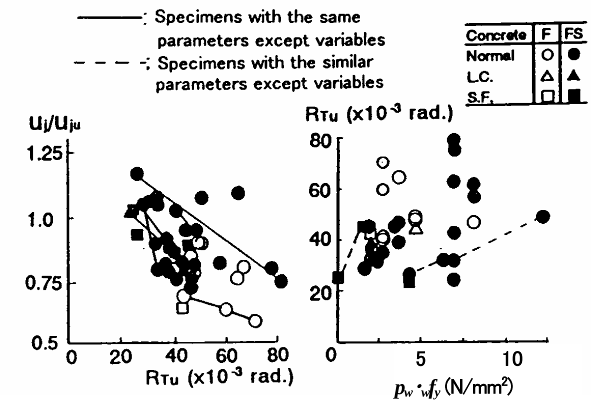

Fig 7 Correlation of R_{Tu} with main parameters

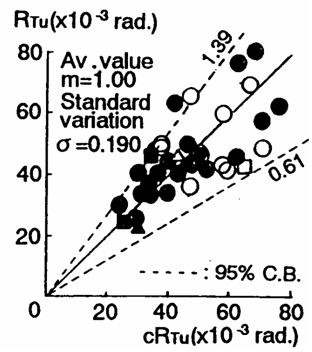

Fig. 8 Comparison of measured (R_{Tu}) and calculated (cR_{Tu}) ultimate story drift angles

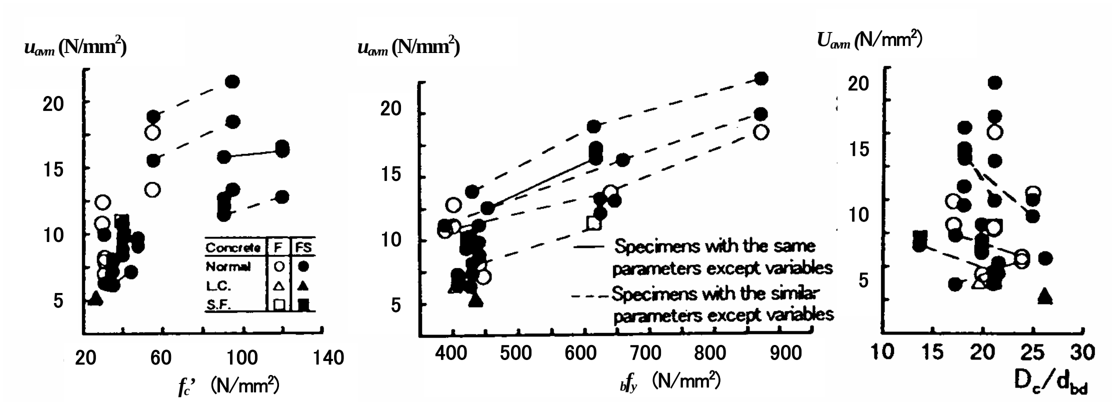

Fig. 9 Correlation of maximum values (u_{avm}) on average bond stress of beam main bars with main parameters

and then considering the other related factors, the prediction equation for the h_{eq} is developed.

5.1 Maximum Values on Average Bond Stress of Beam Longitudinal Bars Passing Through Beam-Column Joints

The measured values of u_{avm} are obtained by applying the Ramberg-Osgood model on the cycle stress-strain relationship of bars. As shown in Fig.9, the correlation of u_{avm} with $D_c/{}_db_d$, ${}_bf_y$ and f_c' are found. As can be seen in this figure, u_{avm} increases with a decrease of $D_c/{}_db_d$ or increase of ${}_bf_y$. The following formula for u_{avm} is obtained by multiple regression analysis considering the effect of above parameters.

$$ {}_cu_{avm} = 0.093k \cdot (D_c/{}_db_d)^{-0.33} \cdot {}_bf_y^{\,0.72} \cdot f_c'^{\,0.31} \qquad (2) $$

where k is a constant given for various concrete type, shown in Table 5. The comparison between measured and calculated values by Eq. (2) was shown in Fig.10 and Table. 3. They show relatively good agreement.

Tab. 5 Values of constants in Eq(2)

Concrete		Constants k
Normal Weight	No Lateral Beam	1.00
	With Lateral Beam	1.65
	Upper Part*	0.91
Light Weight		0.78
Steel Fiber Reinforced		1.01

* Concrete Casting Separates Upper／Lower Parts

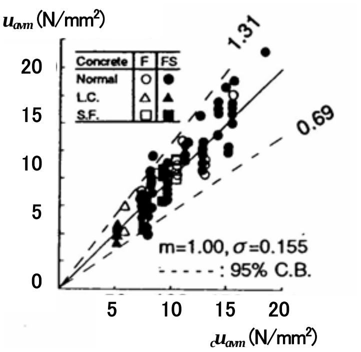

Fig.10 Correlation of measured (u_{avm}) and calculated (${}_cu_{avm}$) maximum values on average bond stress of beam bars in beam－column joints

5.2 Bond Characteristics-Equivalent Viscous Damping Factor Relationship

The h_{eq} of 2nd loop at R_T=1/100, 2/100 and 3/100 rad. is statistically studied by considering the effect of bond stress characteristics by applying the ratio ${}_cu_{avm}/u_b$ and other factors. Where u_b is the average bond stress in beam-column joint, ${}_bf_y \cdot d_{bd}/(2D_c)$, represents the longitudinal reinforcement both at tensile and compressive zones attained yield strength. Fig. 6 showed the relationships between h_{eq} and R_T. The h_{eq} of 2nd loop increased until R_T=3/100 to 4/100 rad. in the case of high strength longitudinal bars but exhibited lower values at $R_T \leqq$ 2/100 rad. compared with the case of normal strength longitudinal bars. The h_{eq} increased up to R_T=2/100 rad. and after that exhibited roughly constant values up to R_{Tu} in the case of normal strength longitudinal bars.

The correlation of h_{eq} with the other parameters are shown in Fig.11 for R_T=2/100 rad. at 2nd cycle. The h_{eq} increased with the increase of the ratio ${}_cu_{avm}/u_b$ but decreased with the increase of ${}_bp_t$ and ${}_bf_y$. If ${}_bf_y \geqq$ 700 N/mm², the h_{eq} exhibited

Tab.6 Values of constants in Eq(3)

R_T[rad.]	k_o	k_1	k_2	k_3
1／100	0.134	0.79	-0.50	-1.48
2／100	0.289	1.13	-0.59	-1.60
3／100	0.296	1.13	-0.31	-1.18

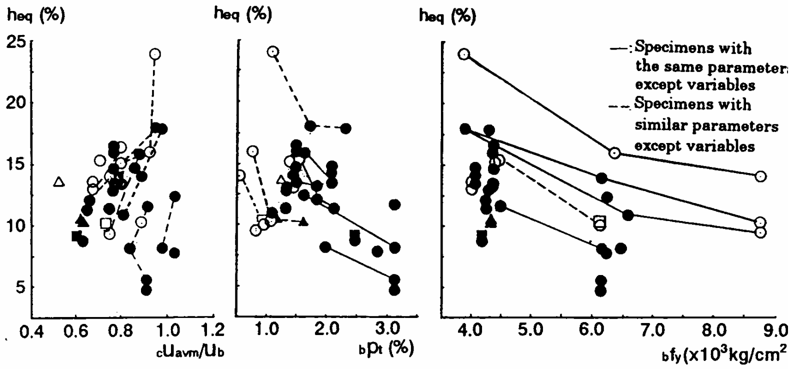

Fig.11 Correlation of h_{eq} (2nd loop at R_T=2/100 rad.) with main parameters

roughly constant values. Considering all the effective factors for h_{eq} is obtained as follows.

$$ {}_ch_{eq} = k_0\left({}_cu_{avm}/u_b\right)^{k_1}\ {}_bp_t^{\,k_2}\left({}_bf_y/400\right)^{k_3} \tag{3}$$

where k_0, k_1, k_2 and k_3 are constants presented in Tab. 6 for R_T=1/100, 2/100 and 3/100 rad.. When ${}_bf_y \leqq 500$ N/mm^2, then $R_T \geqq 2/100$ rad., when ${}_bf_y > 500$ N/mm^2, then $R_T \geqq 3/100$ rad., the h_{eq} are roughly constant up to R_{Tu} for both the cases. If ${}_bf_y \geqq 700$ N/mm^2, ${}_bf_y$ is calculated as 700 N/mm^2.

In Fig.12 and Tab. 3, the correlation between the measured and calculated ${}_ch_{eq}$ by Eq. (3) are shown for R_T=1/100, 2/100 and 3/100 rad.. They are in good agreement.

§6. Restoring Force Characteristics

The restoring force characteristics is determined based on Takeda slip model[8] shown in Fig.13 and using the ${}_ch_{eq}$ evaluation by Eq. (3).

6.1 Skeleton Curves

For the skeleton curves of each element in a subassemblage, the beam skeleton curve (Q_b-R_b) is outlined elastic stiffness and the degradation ratio of yield point stiffness according to authors' equation[7], the beam-column joint panel skeleton curve (Q_p-γ_p) is outlined by model curve[7], and the column skeleton curve (Q_c-R_c) is estimated by flexural deformation and elastic shear deformation. Those relations are converted to Q_c-R_{Tb}, Q_c-R_{Tp}, Q_c-R_{Tc} by coordinate conversion and then the skeleton of Q_c-R_T is finally obtained. The details of this method can be found in references[7].

6.2 Hysteresis Loops

The relation of shaded area, ΔW in Fig.13, with ${}_ch_{eq}$ is obtained as follows [ΔW at ($P_m \cdot D_m$)].

$$\Delta W=\pi \cdot P_m \cdot D_m \cdot {}_ch_{eq} \tag{4}$$

By using the symbols in Fig.13, ΔW is expressed as follows.

$$\Delta W=\{P_x(D_x+X)+(P_m+P_x)(D_m-D_x)-P_m(D_m-X)\}/2 \tag{5}$$

If $k_r=P_m/D_m=P_x/D_x$, $k_s=P_x/(D_x+X)=k_r \cdot D_x/(D_x+X)=P_m \cdot D_x/\{(D_x+X) \cdot D_m\}$,then

$$D_x=(2\Delta W-P_m \cdot X)/\{k_r(X+D_m)-P_m\} \tag{6}$$

If X at (P_m, D_m) and stiffness at decreasing strength (k_d) are given, then the hysteresis loop can be predicted.

6.3 Stiffness at Unloading Path

The correlation of $k_d/{}_ck_T$ to the other factors R_T, f_c', ${}_bp_t \cdot {}_bf_y$ are shown in Fig.14. As shown, $k_d/{}_ck_T$ decreases with increase of R_T or f_c', and $k_d/{}_ck_T$ increases with an increase of ${}_bp_t \cdot {}_bf_y$. Considering all factors, ${}_ck_T$ is formulated by the multiple regression analysis for optional R_T.

$${}_ck_d=\{0.127R_T^{-0.49} \cdot f_c'^{\,-0.30} \cdot ({}_bp_t \cdot {}_bf_y)^{0.49}\} \cdot {}_ck_T \tag{7}$$

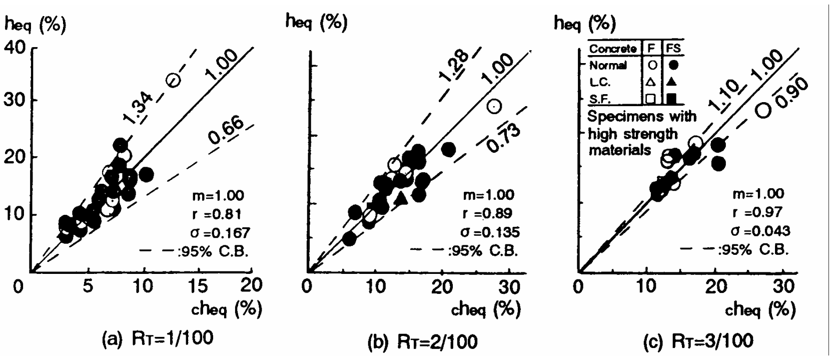

Fig. 12 Correlation of measured (h_{eq}) and calculated (${}_ch_{eq}$) equivalent damping factors

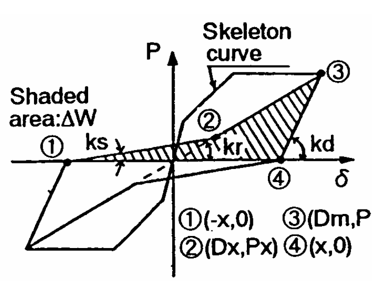

Fig. 13 Hysteresis model (Takeda slip model)

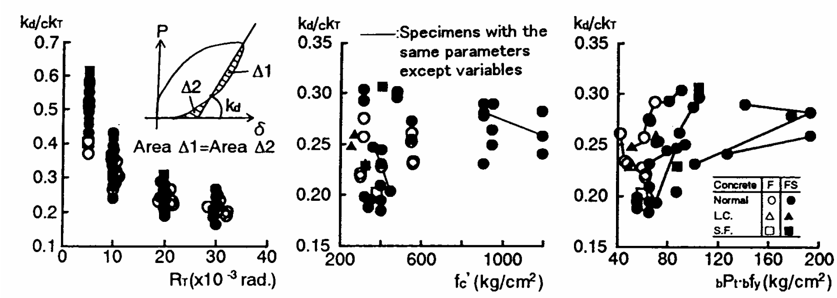

(a) kd/ckT - RT (b) kd/ckT - fc' (RT=2/100rad.) (c) kd/ckT - bPt·bfy (RT=2/100rad.)

Fig. 14 Correlation of *kd/ckT* with main parameters

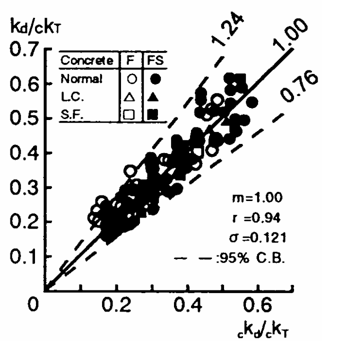

Fig. 15 Correlation of measured (*kd/ckT*) and calculated (*ckd/ckT*) stiffness at decreasing strength

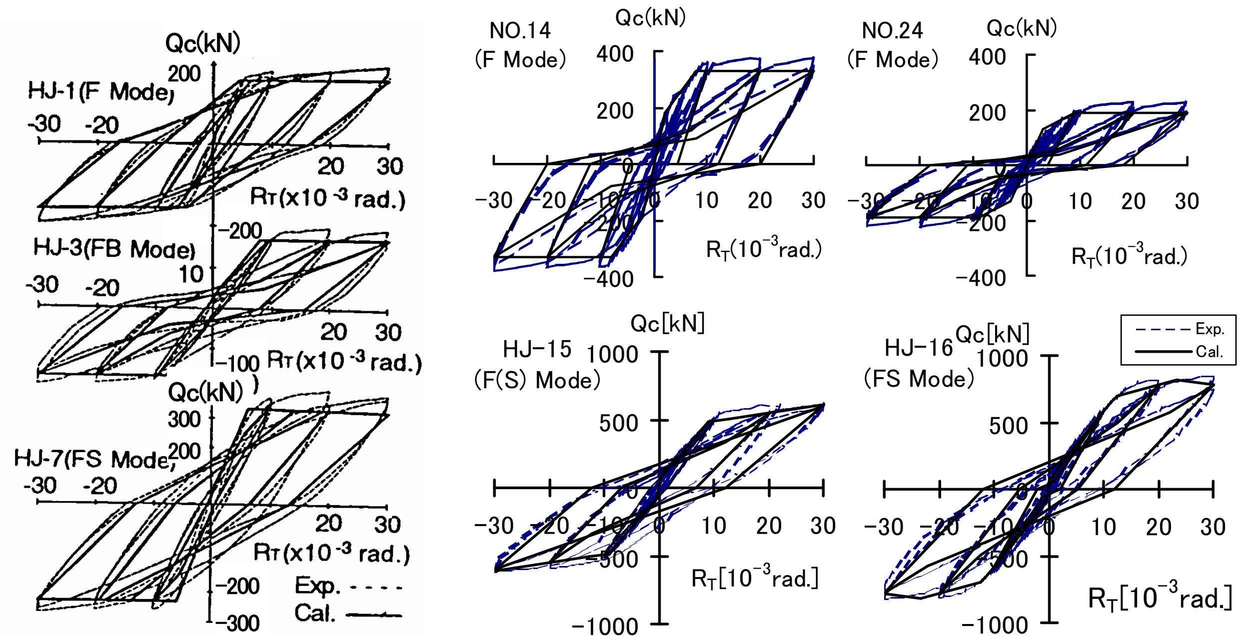

Fig. 16 Comparison of measured and calculated $Q_c - R_T$ restoring force characteristics

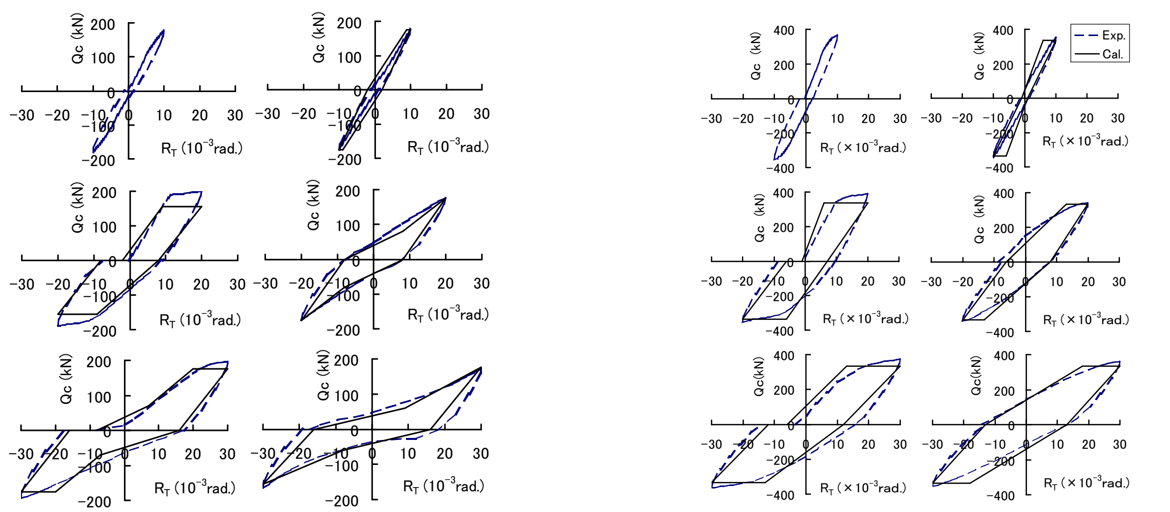

(1) 1st loop (2) 2nd loop

(b) HJ-3 (FB mode)

(1) 1st loop (2) 2nd loop

(b) HJ-7 (FS mode)

Fig.17 Comparison of measured and calculated hysteresis loops at each interstory drift angle of Q_c-R_T relationships

The correlation between the measured and calculated values by Eq. (7) are shown in Fig.15. They are in good agreement.

6.4 Comparison of Measured and Calculated Values of Restoring Force Characteristics

Figure 16 illustrates the measured and calculated restoring force characteristics of Q_c-R_T. As the restoring force characteristics is obtained as described above, the h_{eq} of 1st loop at any interstory drift angle of Q_c-R_T relationships can be obtained. Figure 17 illustrates the measured and calculated hysteresis loops at each interstory drift angle of Q_c-R_T relationships. The calculated values agree well with the measured values even at different conditions.

It is verified that the regression Eqs. (1), (2), (3), (7) and their variables have more than 99% validity.

§7. Conclusions

The following conclusions were drawn from this study;

(1) The anchorage capacity of beam longitudinal bars passing through the interior beam-column joint affects the energy absorption of a frame.

(2) The plastic deformation performance of subassemblages of a beam yielding frame is greatly effected by the joint input shear force level and the amount and strength joint shear reinforcement.

(3) A method to estimate restoring force characteristics of the subassemblages that takes the above effects into account was developed. Across a range of conditions, the results calculated by our proposed method closely predicted the ductility performances and hysteresis characteristics measured in the test subassemblages using normal-to high-strength materials.

References

1) Leon, R.J., "Anchorage Requirements in Interior Beam-Column Joints", *9th World Conference on Earthquake Engineering*, paper E08-05, Tokyo/Kyoto, 1988.

2) Kaku, T.and Asakusa, H., "Bond and Anchorage of Bars in Reinforced Concrete Beam-Column Joints," *ACI SP-123*, American Concrete Institute, pp.401－423, 1991.

3) Teraoka, M., Kanoh, Y., Hayashi, K. and Sasaki, S., "Effect of Bond Characteristics of Beam Main Rebar passing through Beam-Column Joints on Hysteretic Restoring Force Characteristics of RC Interior-Subassemblages", *Proceeding of the Japan Concrete Institute*, Vol.14, No.2, pp.425-430, 1992 (in Japanese).

4) Teraoka, M. Kanoh, Y., Hayashi, K. and Sasaki, S., "BEHAVIOR OF INTERIOR BEAM-AND-COLUMN SUBASEEMBLAGES IN AN RC FRAME", *ASCE, High Strength Concrete, First International Conference*, pp.93-108, 1998.

5) Teraoka, M., Kanoh, Y., Sasaki, S., Fujiwara T. and Hayashi, K., "Study on the Shear Strength of RC Interior Beam-Column Joints," *Journal of Structural Engineering*, *AIJ*, Vol. 37B, pp.379－392, 1991 (in Japanese).

6) AIJ, *Standard for Structural Calculation of Reinforced Concrete Structures*, Architectural Institute of Japan, 1988 (in Japanese).

7) Teraoka, M., Kanoh, Y., Sasaki, S. and Hayashi, K., "An Estimation of Ductility in Interior Beam-Column Subassemblages of Reinforced Concrete Frames," *Journal of The Society of Material Science Japan*, Vol. 45, No. 9, pp.1033－1041, 1996 (in Japanese).

8) Eto, H. and Takeda, T., "Elasto-plastic Earthquake Response Frame Analysis of Reinforced Concrete Structures," *Summaries of Technical Papers of Annual Meeting, AIJ*, pp.1507－1508, 1977 (in Japanese).

Appendix Ⅰ Notations

The following symbols are used in this paper:

a = nominal cross sectional area of reinforcing bar (mm^2);
a_t = total area of tensile reinforcement in beam;
b_b, b_c = widths of beam and column (mm);
D_b, D_c = depths of beam and column (mm);
d_{bd} = bar diameter of longitudinal reinforcement in beam (cm);
E = Young's modulus of concrete at l/4 f_c' (N/mm^2)
F, FB, FS = failure mode types in the subassemblage;
f_0 = axial compressive stress in column (N/mm^2);
f_c' = compressive strength of concrete (N/mm^2);
f_y = yield strength of reinforcing bar (N/mm^2);
${}_bf_y$ = yield strength of longitudinal reinforcement in beam

(N/mm^2);
$_wf_y$ = yield strength of transverse reinforcement in joint (N/mm^2);
H = story height (mm);
h_{eq} , $_ch_{eq}$ = measured and calculated equivalent damping factors;
j_c = 7/8th of effective depth of column (mm);
k, k_0, k_1, k_2, k_3 = Values of constant in eq.(2) and eq.(3);
k_d, $_ck_d$ = measured and calculated stiffness at unloading path in subassemblage;
$_ck_T$ = elastic stiffness in subassemblage under horizontal loading;
L = span length (mm);
N = axial force in column;
$_bp_t$, $_cp_t$ = tensile reinforcement ratios in beam and column;
p_w = transverse reinforcement ratio;
Q_c = story shear force;
Q_{cby}, Q_{cbu} = measured and calculated story shears at beam flexural yielding;
Q_{cm}, Q_{cbm} = measured and calculated story shears at maximum load;
R_T = interstory drift angle;
R_{Ty}, R_{Tm} = measured interstory drift angles at beam flexural yielding and maximum load;
R_{Tu}, $_cR_{Tu}$ = measured and calculated ultimate interstory drift angles;
$u_b = d_{bd} \cdot {}_bf_y/(2D_c)$ = average bond stress in beam-column joint considering the beam longitudinal reinforcement both at tensile and compressive zones attained yield strength;
u_{avm} , $_cu_{avm}$ = measured and calculated maximum values on average bond stress of beam main bar in joint;
v_{jc}, $_cv_{jc}$= measured and calculated shear cracking stresses in joint;
v_{jm} = measured maximum joint shear stress;
v_{ju} = calculated ultimate joint shear strength according to the equation proposed by the authors (1991)[5];
v_n = nominal shear stress of beam-column joint at beam flexural yield capacity according to approximate equation of AIJ(1988);
v_n/v_{ju} = joint input shear stress level;
$\mu = d_{bc} \cdot {}_bf_y / (D_c \cdot \sqrt{f'_c}\,)$ = bond index; and
$\eta_0 = f_o / f_c'$ = axial compression ratio of column.

Masaru Teraoka

short comment A method to estimate restoring force characteristics of the subassemblages of R/C frames using normal- to high-strength materials was developed. I want to apply this method to structural design for super-high-rise apartment house buildings (more over 60 stories)